Journal of Membrane Science 392–393 (2012) 1–8

Contents lists available at SciVerse ScienceDirect

Journal of Membrane Science

journal homepage: www.elsevier.com/locate/memsci

On the enhanced drag force induced by permeation through a filtration membrane

Guy Z. Ramon[1], Eric M.V. Hoek*

Department of Civil & Environmental Engineering and California NanoSystems Institute, University of California, Los Angeles, CA 90095, USA

ARTICLE INFO

Article history:
Received 23 June 2011
Received in revised form
21 September 2011
Accepted 21 October 2011
Available online 17 November 2011

Keywords:
Sphere drag correction
Particle deposition
Membrane separation
Analytical solution

ABSTRACT

Permeation drag is the predominant cause for particle deposition onto filtration membranes, and it is known that at close approach to the membrane surface this force may greatly exceed the Stokes drag in an unbounded fluid. Herein, the hydrodynamic interaction between a sphere and a permeable wall is re-visited within the framework of the lubrication approximation with the goal of deriving an analytical solution. A closed-form analytical solution is found, based on a perturbation expansion in terms of the scaled permeability, which is considered a small parameter. Numerical calculations of the drag force on the sphere agree perfectly with numerical results available in the literature, as do analytical model results within a range of validity which is affected by the particle size and membrane permeability. Specifically, the presented calculations have been framed in the context of the low permeabilities and colloidal particle sizes representative of commercial membrane separations in current use. Results illustrate that for reverse osmosis and nanofiltration membranes, the hydrodynamic interaction is practically identical to that of an impermeable wall, while for ultrafiltration membranes the drag is substantially reduced; an analogous trend is observed for increasing particle sizes. The approximate solution derived herein offers a simple and direct means of performing hydrodynamic force calculations in particle–membrane systems.

1. Introduction

It is well-known that a sphere approaching a solid wall interacts with it hydrodynamically, such that the drag force experienced by the sphere is greatly enhanced over that predicted by Stokes' law in an unbounded fluid. For the case of a sphere translating in the direction perpendicular to the plane wall, this problem was first fully treated by Brenner [1], who solved the equations of creeping motion using a stream-function formulation in bi-polar coordinates. Increased drag is also exerted on a sphere translating parallel to a plane wall, due to hydrodynamic interactions; however, this case is not considered herein (the interested reader is referred to, e.g., Ref. [2]).

In the considered case, that of the perpendicular approach of a sphere to the wall, the increased force is due to 'squeezing' of a liquid film between the wall and the approaching particle; at close approach, the pressure required to drive this flow becomes exceedingly large, resulting in a force on the particle which opposes its motion. The solution diverges at contact, paradoxically predicting that an infinite force would be required for the sphere to contact the surface. If, on the other hand, the wall is permeable to the surrounding fluid, this opposing force is significantly reduced since the fluid may now flow through the wall as well, as first shown by Goren [3], who also predicted that there must be a finite force at 'contact'. Goren's analysis results in a set of non-linear difference equations, which must be solved numerically; some tabulated data are provided for a range of scaled permeabilities which, at their lowest range, is comparable with a system comprised of micrometer-size particles and microfiltration membranes. Clearly, this approach is not easily accessible for consideration of membrane–particle systems representative of modern capabilities. It is also important to note that implicit to these models and, indeed, the present work, is the assumption that the wall is uniformly permeable and, hence, any local effects arising from the flow field in the vicinity of pores are ignored. This problem has been extensively treated in the literature (see, for example, Refs. [4–7]). Exact determination of this scale separation limit is complicated, since the 'pore-scale' analysis is independent of the permeability which, in turn, is the defining characteristic of a 'macro-scale' analysis for the permeable wall case. However, according to Yan et al. [4], for a particle-to-pore ratio of 10 and a separation of one particle radius, the correction coefficient to the perpendicular drag exerted on the particle deviates from that for the non-permeable case by 10%; the deviation from the 'macro-scale' permeable case is expected to be even smaller. This

* Corresponding author. Tel.: +1 310 206 3735; fax: +1 310 206 2222.
E-mail address: emvhoek@ucla.edu (E.M.V. Hoek).
[1] Present address: Department of Mechanical & Aerospace Engineering, Princeton University, Princeton, NJ 08544, USA.

0376-7388/$ – see front matter © 2011 Elsevier B.V. All rights reserved.
doi:10.1016/j.memsci.2011.10.056

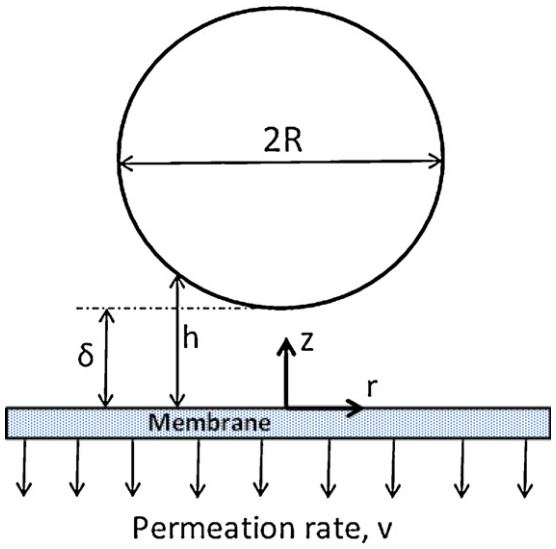

Fig. 1. Schematic illustration of the sphere-membrane geometry.

example may serve as an approximate measure of the scale separation appropriate for the type of 'macro-scale' analysis considered in this paper.

Particle deposition onto filtration membranes is primarily caused due to permeation drag, i.e., the force exerted on the particle by the flow of water permeating through the membrane. Most importantly, this enhanced drag is dependent on the membrane permeability, becoming greater as the membrane becomes less permeable. Therefore, when a force balance approach is used to model particle deposition, a drag correction factor must be used to accurately account for the permeation-induced force component. For example, Chellam and Wiesner [8] used Brenner's analytical solution to account for the increased permeation drag; this expression does not, however, account for the permeability of the membrane and so its validity for use in such a case must be established. Goren's analytical approximation for the force at contact has been used by Knutsen and Davis [9] to describe particle dynamics at the membrane surface. More recently, Goren's tabulated numerical data have been numerically approximated and employed for force balance calculations in a number of deposition studies [10–13]. This approach has been shown to produce reasonable predictions of deposition rates as well as conditions leading to reversible deposition.

While it is evident that a physically realistic drag correction for particle deposition in membrane processes must account for the membrane (wall) permeability, making such calculations requires the use of extrapolations based on tabulated data or numerically solving a set of difference equations, as formulated by Goren [3]. In this paper, the problem of a sphere interacting hydrodynamically with a permeable wall is re-visited with the goal of deriving a closed-form, approximate analytical solution, assessment of its accuracy compared with numerical calculations and previously published results and, finally, evaluation of the drag force for relevant membrane permeabilities and representative particle sizes.

2. Model formulation

Consider a spherical particle of radius R, immersed in an incompressible fluid with constant viscosity, μ, in the vicinity of a permeable membrane surface as depicted schematically in Fig. 1. The membrane is assumed to be uniformly permeable, i.e., local effects in the vicinity of pores are ignored. The fluid may be pressurized so as to induce permeation through the membrane, and this background pressure, p_∞, is taken to be everywhere uniform far from the sphere. It is further assumed that the sphere may not rotate, but may be subjected to translational motion.

The primary interest here is with the hydrodynamic interaction at close proximity of the sphere to the wall; hence, the flow within the gap between the sphere and the wall may be described using the classical 'lubrication approximation', also known as the 'long-wavelength approximation' (for a rigorous derivation the reader is referred to Refs. [14,15]). Essentially, within the lubrication framework, it is assumed that two disparate spatial scales exist, namely that the characteristic gap length-scale is much shorter than the longitudinal length-scales (radial direction, in the axisymmetric case considered here); therefore, changes over the longer length scale occur much slower than over the short scale, and so longitudinal gradients may be considered very small at leading order.

Under this approximation, the equations of motion are reduced to

$$\frac{\partial p}{\partial r} = \mu \frac{\partial^2 u}{\partial z^2}, \tag{1}$$

$$\frac{\partial p}{\partial z} = 0, \tag{2}$$

and the continuity equation

$$\frac{1}{r}\frac{\partial}{\partial r}(ru) = -\frac{\partial w}{\partial z}, \tag{3}$$

in which u, w are the velocity components in the r and z directions, respectively, and p is the excess pressure (relative to the background pressure, p_∞).

The boundary conditions used herein are no-slip of the tangential velocity on the wall and sphere,

$$u(0) = u(h) = 0, \tag{4}$$

where $h = h(r)$ is the gap width between the sphere surface and the wall, which may be approximated as

$$h = \delta + \frac{r^2}{2R} + O(r^4), \tag{5}$$

with δ denoting the minimum distance between the sphere and the wall (see Fig. 1).

The boundary conditions on w, the z component of the velocity, are

$$w(h) = -v_s, \tag{6}$$

at the surface of the sphere, with v_s denoting the velocity of the sphere and

$$w(0) = -\frac{k^*}{\mu l}\left(p_{z=0} + p_\infty - p_p\right) = -v, \tag{7}$$

at the membrane surface, in which p_p is the pressure in the permeate side of the membrane, k^* is the Darcy permeability and l is the membrane thickness. Assuming that the permeate pressure is atmospheric, and noting that under the lubrication approximation, the pressure does not vary with z (see Eq. (2)), the velocity at the boundary may be related directly with the pressure at any radial location, viz.

$$w(0) = -\frac{k}{\mu}(p_\infty + p) = -v, \tag{8}$$

where $k = k^*/l$. Note that traditionally the permeability has the dimensions of [m^2], while in the present analysis the permeability is taken per unit thickness of the membrane, thus having the

dimensions of [m]. The derivation procedure is now straightforward and Eq. (1) may be integrated twice using Eq. (4), yielding

$$u = \frac{1}{2\mu}\frac{\partial p}{\partial r}\left(z^2 - hz\right). \tag{9}$$

Next, this velocity profile is substituted into Eq. (3) and is integrated again across the gap, resulting in

$$w(h) - w(0) = \frac{1}{12\mu r}\frac{\partial}{\partial r}\left(rh^3\frac{\partial p}{\partial r}\right). \tag{10}$$

Substituting the Eqs. (6) and (8) into Eq. (10) results in the following second-order ODE for the pressure within the gap:

$$-v_s = \frac{1}{12\mu r}\frac{d}{dr}\left(rh^3\frac{dp}{dr}\right) - \frac{k}{\mu}(p_\infty + p), \tag{11}$$

with the boundary conditions

$$\frac{dp}{dr} = 0 \quad \text{at} \quad r = 0, \tag{12}$$

from symmetry considerations and

$$p = 0 \quad \text{at} \quad r \to \infty, \tag{13}$$

the far-field pressure. Note that the pressure here is that in excess of the background pressure, p_∞, hence it is assumed to decay to zero far from the sphere.

The derived equation describes the dependence of the excess pressure on the motion of the sphere and the wall permeability. On the approach of the particle to the wall, pressure is built up within the gap as water is squeezed out through a smaller aperture. The additional term accounting for wall permeation will tend to reduce the pressure in the gap, as first noted by Goren [3], since the fluid has an additional path through which to flow.

2.1. Asymptotic solution

In order to facilitate the asymptotic analysis, Eq. (11) is recast into non-dimensional form by scaling all lengths with the sphere radius, R, the velocity scale is taken as the background permeation rate, $v = kp_\infty/\mu$ and the pressure is scaled using the viscous stress, $\mu v/R$. The resulting equation is

$$-V_s = \frac{1}{12\eta}\frac{d}{d\eta}\left(\eta H^3\frac{dP}{d\eta}\right) - (1 + \alpha P), \tag{14}$$

where $\eta = r/R$, $V_s = v_s/v$, and $H = \Delta + \eta^2/2$, where $\Delta = \delta/R$. The boundary conditions given by Eqs. (12) and (13) are unchanged.

Making use of the fact that for characteristic membrane permeabilities, $\alpha = k/R \ll 1$, an approximated solution may be sought through an asymptotic expansion in terms of α:

$$P = P_0 + \alpha P_1 + \alpha^2 P_2 + \ldots. \tag{15}$$

Substitution of Eq. (15) into Eq. (14) results in a set of perturbation problems which are given here to first order in α, as follows:

$$\text{At} \quad O(1), \quad \frac{1}{12\eta}\frac{d}{d\eta}\left(\eta H^3\frac{dP_0}{d\eta}\right) = -V_s, \tag{16}$$

the solution to which is readily found to be

$$P_0 = \frac{12(V_s)}{(2\Delta + \eta^2)^2}, \tag{17}$$

which, up to a choice of scaling and inclusion of the background permeation, is the classical lubrication solution [14].

Proceeding to the next order, at $O(\alpha)$ we have

$$\frac{1}{12\eta}\frac{d}{d\eta}\left(\eta H^3\frac{dP_1}{d\eta}\right) - P_0 = 0. \tag{18}$$

The solution to this ODE provides the first order correction accounting for the permeable wall:

$$P_1 = -\frac{48(V_s - 1)}{\Delta(2\Delta + \eta^2)^3}. \tag{19}$$

So that the solution for the pressure field is given, to first order in α, as

$$P(\eta) = \frac{12(V_s)}{\left(2\Delta + \eta^2\right)^2} - \frac{48(V_s - 1)\alpha}{\Delta\left(2\Delta + \eta^2\right)^3} + O(\alpha^2). \tag{20}$$

Additional correction terms, up to $O(\alpha^6)$, have been calculated and are given in Appendix A; higher order terms may be obtained, in principal, becoming increasingly cumbersome.

From inspection of Eq. (14) it may be inferred that the expansion in powers of the small parameter α is expected to be accurate as long as $\Delta \gg \alpha$; when the minimal gap separation approaches $O(\alpha)$, this must be taken into account in the asymptotic expansion, since Eq. (14) then becomes singular as $r \to 0$. Calculating higher-order correction terms somewhat increases the accuracy however at a very slow rate of convergence (see Appendix B).

2.2. The drag force

The main result of the lubrication analysis is the pressure distribution within the film. In the present case, this enables the calculation of the force exerted on the sphere. For lubrication type problems, the contribution of viscous stresses is negligible compared with the pressure. The force on the sphere is therefore given by

$$F_D = 2\pi\int_0^\infty \eta\, p(\eta)d\eta. \tag{21}$$

Substituting Eq. (20) and performing the integration yields

$$F_D = 6\pi(V_s - 1)\left(\frac{1}{\Delta} - \frac{\alpha}{\Delta^3}\right) + O(\alpha^2), \tag{22}$$

or, in dimensional form:

$$F_D = 6\pi\mu R(v_s - v)\left(\frac{R}{\delta} - \frac{kR^2}{\delta^3}\right) + O(k^2). \tag{23}$$

This force may be regarded (in the lubrication limit), as the correction to the Stokes drag force on a sphere, as defined by Brenner [1]. Setting the background permeation velocity, v, to zero results in an expression which may be directly compared with Goren [3] and Brenner's [1] treatment of a sphere translating through a quiescent fluid, approaching a permeable and non-permeable wall, respectively.

The present analysis allows for both a translational velocity imposed on the sphere by some external force as well as a background permeation. If no relative motion exists between the sphere and surrounding fluid, Eq. (22) predicts no increased drag force on approach; this is since there is no liquid 'squeezing' and therefore no pressure build-up at the sphere's leading edge. The two other limiting cases, i.e., a sphere translating in a quiescent fluid ($v = 0$) and a stationary sphere immersed in a background permeation-induced flow ($v_s = 0$) are identical in magnitude, to within a choice of scaling, and opposite in sign. Given a constant force acting on the sphere, its velocity should decrease on approach to a non-permeable surface. In the case of membrane filtration, the situation is far more complex since this force is dependent upon the permeation rate itself, such that the permeation rate and the translational velocity of the particle are not equal. Though interesting in itself, this dynamic problem is beyond the scope of the present analysis. In the case considered herein, the situation of interest is that of a stationary sphere held at some equilibrium position by a balance

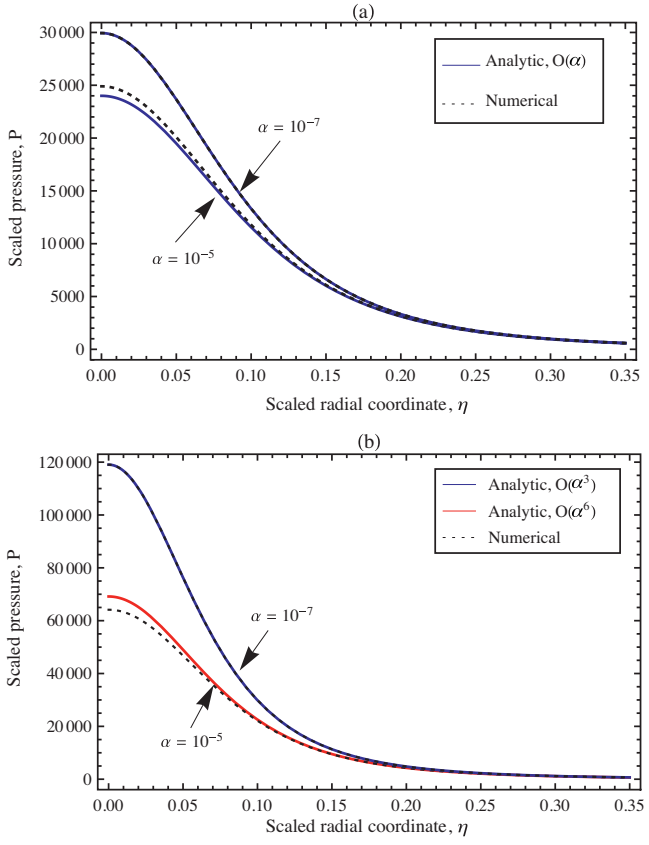

Fig. 2. Radial distribution of the scaled pressure, P, at two different separation distances. (a) $\Delta = 0.01$. (b) $\Delta = 0.001$. Numerical calculations (dotted lines) are compared with analytical solutions with varying number of higher-order correction terms.

of forces arising from surface interactions (XDLVO) and the permeation drag, enhanced by the presence of the membrane (see, for example, [10,11]).

The derived analytical expression given by Eq. (22) is a main result of the present study as it enables a simple straightforward calculation of the hydrodynamic force exerted on a sphere near a permeable wall. It also generalizes previous studies by including a background permeation flow. In the following section some results are presented, which illustrate both the utility and limitations of this approximation for a parameter range relevant to membrane separation.

3. Results and discussion

Calculations have been carried out for the pressure distribution as a function of the parameters governing the problem, namely the scaled permeability, $\alpha = k/R$, and the scaled separation distance, $\Delta = \delta/R$. The radial pressure distribution, in scaled form, is plotted in Fig. 2, using both the numerical solution of Eq. (14) as well as the analytical approximation (Eq. (20) supplemented, where necessary, by additional terms to various orders of accuracy, as given in the appendix). As may clearly be seen, the pressure build-up is particularly dramatic at the regions of closest approach, beyond which it declines rapidly. As already mentioned in the previous section, it is this pressure which creates an increased drag force on the sphere. The accuracy of the approximations is here shown to depend strongly on both the scaled separation distance, Δ, and permeability, α; when $\Delta = 0.01$, the first-order correction given by Eq. (20) is virtually indistinguishable from the numerical solution for $\alpha = 10^{-7}$, but shows some visible deviation for $\alpha = 10^{-5}$ (see

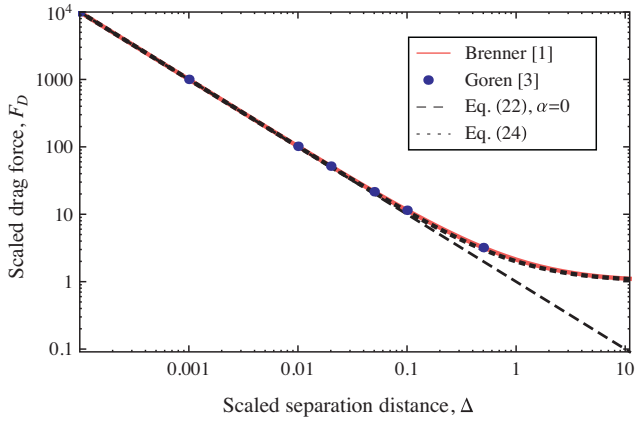

Fig. 3. Scaled drag force, F_D, calculated using the lubrication solution with $\alpha = 0$, compared with 'exact' solutions of the Stokes equation [1,3].

Fig. 2a). At a closer position, $\Delta = 0.001$, a higher-order approximation is required, e.g., for $\alpha = 10^{-7}$ the $O(\alpha^3)$ approximation provides an excellent depiction of the pressure distribution, while at $\alpha = 10^{-5}$ even the sixth-order term deviates visibly in the region of closest approach (for $\eta < 0.05$), where the asymptotic expansion is no longer valid. It should also be noted, that even the numerical solution becomes increasingly 'stiff' at close approaches, since the equation itself possesses an inherent singularity at the origin when the sphere is in contact with the surface.

A slight deviation in the pressure distribution may translate into a significant error once the force on the sphere is calculated, as it is an integral over the pressure distribution. Some representative calculations illustrating the accuracy of the analytical solutions at various orders of approximation have been made and are given in Appendix B. Higher permeabilities and closer separation distances require more terms to be added in the asymptotic approximation if the force is to be calculated at close approach; for example, with a permeability of $\alpha = 10^{-5}$, the analytical solution at $O(\alpha^6)$ is accurate up to a separation of $\Delta \approx 0.005$, while at $\alpha = 10^{-8}$ the first-order correction is sufficiently accurate up to a separation of $\Delta \approx 0.0002$.

Next, the lubrication-based calculations are compared with the 'exact' analytical solution derived by Brenner [1] for a non-permeable wall and Goren's [3] tabulated values obtained through a numerical solution. For completeness, it must be noted that the lubrication approach can only predict the additional force on the sphere due to the 'squeezing' effect which only comes into play in the vicinity of a boundary. Far from the boundary, this additional force is not present and so the predicted lubrication force is zero, and it does not account for the force on a sphere in an unbounded fluid (the Stokes drag). Therefore, when comparing this force to the full solution of the Stokes equation, such as that derived by Brenner [1], a correction accounting for this far-field drag force may be added. For example, in the case of a sphere translating towards an impermeable surface ($\alpha = 0$), the scaled drag force will be

$$F_D = 6\pi V_s \left(1 + \frac{1}{\Delta}\right). \tag{24}$$

Fig. 3 illustrates the validity of the lubrication approach; when the far-field Stokes drag is not accounted for, a clear deviation from the 'exact' solution is seen, beginning at $\sim\Delta = 0.1$ and growing with increased separation. Indeed, when $\Delta \gg 1$ the excess pressure reduces to zero as does the increased drag force because the sphere is too far from the wall to interact with it. The drag computed from the 'exact' solution [1,3] would decay to 1, that is, the Stokes drag. When this is accounted for, the solutions overlap and the simple expression given by Eq. (24) may be accurately used for calculating the drag near an impermeable wall.

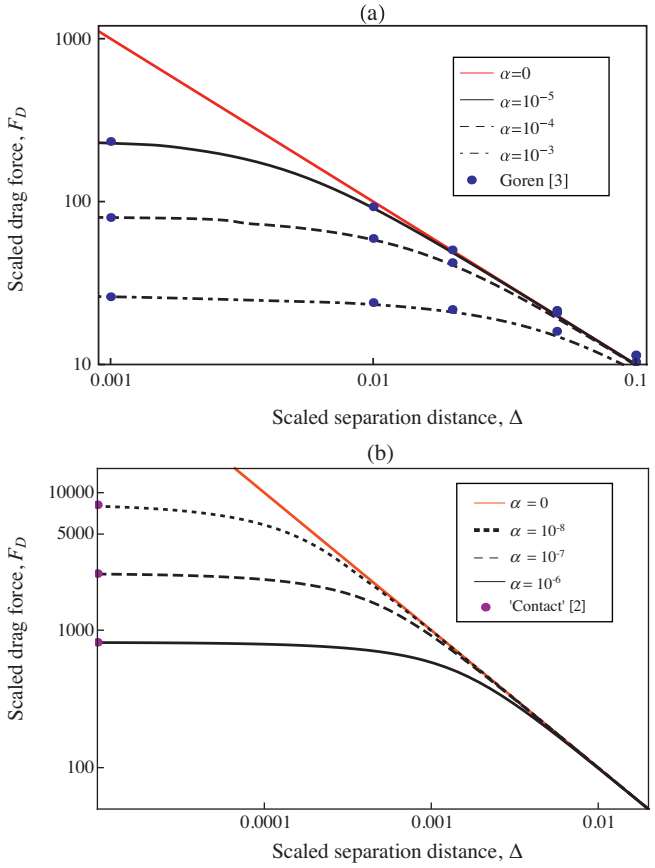

Fig. 4. Scaled drag force, F_D, as a function of the scaled separation distance, $\Delta = \delta/R$, calculated for various values of the scaled permeability, $\alpha = k/R$. Calculations shown are made using a numerical solution of Eq. (14). (a) Comparison with Goren's calculations [3]. (b) Calculation made for range of permeabilities representative of membrane separation. Also shown are the calculated values at 'contact', based on Eq. (25) [3].

In the case of a permeable wall, numerical calculations have been made for the permeability range $\alpha = 10^{-3} - 10^{-8}$, and are shown in Fig. 4. The lower range of permeabilities is compared with the calculations reported by Goren [3], showing excellent agreement (Fig. 4a); the calculation is then extended to lower permeabilities, which were not reported in Goren's paper (Fig. 4b). Furthermore, Fig. 4b also includes points calculated from Goren's expression for the drag force at 'contact' which, in the current notation, may be written as [3]

$$F_{contact} = \left(\frac{2}{3\alpha} + 1.072^2\right)^{1/2}. \quad (25)$$

This approximation generally falls within ~5% of our numerical solution for low permeabilities, with a greater deviation as the permeability decreases. It must be noted that in a physically realistic situation, the forces calculated at such close separation are most likely to be inaccurate by neither approach, nor is it likely to have true 'contact', in the sense which it is considered in the derived model. This issue is beyond the scope of the present study but will be considered briefly in a later section.

We now consider the physical significance, in dimensional form, of the scaled parameters used in the calculations. The scaled force may be written as $F_D = f(\alpha, \Delta)$ and, as already mentioned, is the correction factor to the Stokes drag force on a sphere. For membrane separation applications, the order-of-magnitude range of permeabilities which may be considered is $k \approx 10^{-12}$ m for MF membranes and down to $k < 10^{-14}$ m for reverse osmosis (RO) membranes.

Table 1
Representative RO, NF and UF membranes and their permeabilities.

	Seawater RO		'High flux' RO	
Membrane	SWC4	SWHR	BW30	ESPA
Permeability, k (m)	2.3×10^{-15}	4.2×10^{-15}	1×10^{-14}	1.8×10^{-14}
	NF	UF		
Membrane	NF270	EW	MX50	MX500
Permeability, k (m)	5×10^{-14}	1.8×10^{-13}	9.4×10^{-13}	3.3×10^{-12}

A representative compilation of values for some commercial UF, NF and RO membranes is given in Table 1. Considering particle sizes in the range 10 nm–1 μm, this corresponds with the range $10^{-3} < \alpha < 10^{-8}$. Note, however, that a value of $\alpha \approx 10^{-3}$ would correspond with, for example, a MF membrane and a 10 nm particle; for such a system, the particle radius would be comparable with pore dimensions and so the framework of the present analysis is not expected to be accurate. As already discussed briefly in the introduction, when the particle size is 10 times larger than the pore size, this deviation is not expected to be significant. We note that, in general, this 'pore-scale' effect is expected to reduce the lubrication 'resistance' force, since there is a reduction in the solid surface producing the gap and, hence, the 'squeezing' of fluid which creates the pressure build-up and the resulting force. The scaled separation, $\Delta = \delta/R$, which would correspond with a distance approaching molecular length-scales (on the order of 1 nm, say) may then be estimated to be $\Delta = 0.001$ for a particle with a radius of 1 μm (which may be considered as representative of bacteria). With these orders of magnitude in mind, calculations have been made for the increased permeation drag in the vicinity of some representative commercial membranes, for particle sizes ranging between $R = 0.1$ and 2 μm. Fig. 5 summarizes these calculations, and also illustrates the range of accuracy of the approximate solution. We note that for the highest permeability membrane used in these calculations (MX500), the scale separation mentioned earlier may not be strictly met for a particle radius of 100 nm (the pore radius of this membrane is estimated to be 25 nm); nonetheless, these calculations are illustrative of the reduced force on the particle, compared with that acting in the vicinity of an impermeable wall.

Note that on a logarithmic plot, the drag force for a non-permeable wall, which scales as $1/\delta$, appears as a straight line; deviation from this is observed when the induced permeation through the wall reduces the increased drag. At the low range of permeabilities representative of RO and NF membranes, the departure from the behavior of a non-permeable system is rather small; in fact, the additional drag predicted in the presence of an RO membrane is practically identical to that of a non-permeable surface, up to a scaled separation of $\Delta \sim 0.0005$. This separation distance is physically nonsensical for a particle with $R < 1$ μm. Another interesting feature is that larger particles are more strongly affected by the wall permeability, while small particles, even at higher permeabilities, interact with the membrane as though it were a non-permeable surface. However, in general, for higher permeabilities and larger particles, the deviation of the enhanced drag from that of the non-permeable wall (and the Stokes drag) may be substantial and should be accounted for.

As a final remark, while it has been nearly forty years since this topic was first explored, the hydrodynamic interaction between particles and surfaces remains an active research topic. Experimental and theoretical probing of close-range interactions are currently being pursued utilizing state-of-the-art experimental techniques such as atomic force microscopy (AFM) and the surface

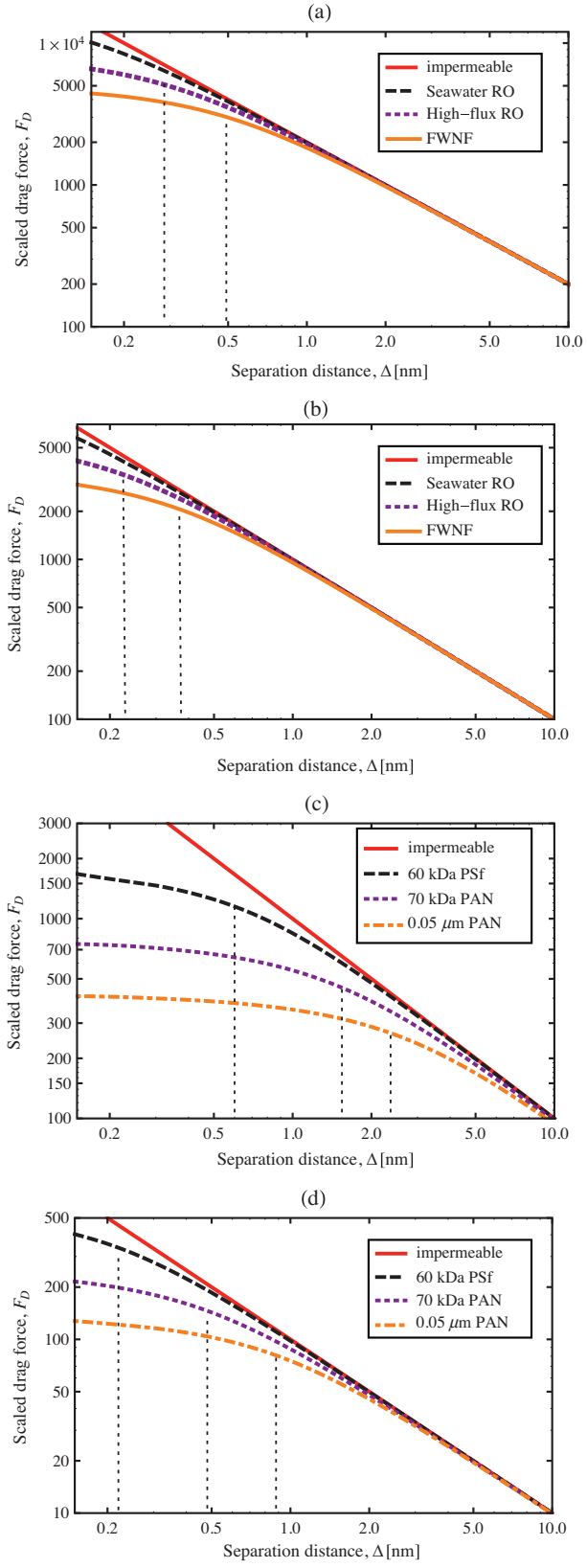

Fig. 5. Scaled drag force, F_D, as a function of the separation distance, δ (in nm), calculated for permeabilities (k) representative of various membrane separation processes. (a) Seawater RO (SWRO), High-flux RO and Freshwater NF (FWNF), $R = 2$ μm, (b) RO/NF, $R = 1$ μm, (c) UF, $R = 1$ μm and (d) UF, $R = 100$ nm. Vertical lines are a guide to the eye, indicating approximate separation at which the analytical solution at $O(\alpha^6)$ deviates from the numerical calculation.

force apparatus (SFA). These, combined with molecular dynamics simulations, Lattice-Boltzmann simulations and continuum approaches have consistently illustrated the accuracy of the lubrication approximation down to molecular length-scales. However, at close approach surface properties become of fundamental importance for accurately describing the interaction. In particular, effects of roughness and surface energy (hydrophobicity) have been subject to many recent studies [16–20]. In the context of particle deposition onto separation membranes, the quantitative effect of these surface properties remains elusive; nevertheless, some analogies may perhaps be drawn with existing data on non-permeable surfaces. Such possible extensions are left for future work.

4. Concluding remarks

The hydrodynamic interaction between a sphere and a permeable wall was studied within the framework of the lubrication approximation. A closed-form analytical solution was derived and the calculated drag force on the sphere agreed well with numerical results for permeable and non-permeable walls. The accuracy of the asymptotic solution as well as its range of validity has been demonstrated, illustrating the utility of the analytical approximation. In contrast with previous related studies, where numerical analysis of the problem has been performed, the approximate solution derived herein offers a simple and direct means of performing hydrodynamic force calculations for particle-membrane systems.

For the low permeabilities and colloidal particle sizes typical of ultrafiltration membranes in current use, the drag force may be substantially lower than that predicted for a non-permeable wall, but significantly higher than that predicted by the Stokes drag. Interaction with low permeability membranes, such as those used in RO desalination applications, is practically identical to that of a non-permeable wall down to extremely close separation distances; the same behavior is observed for nano-particles, even in the vicinity of more permeable membranes used for UF. Future extensions to this model may include particle rotation, such as that expected in a parallel shear flow and effects arising from surface roughness and hydrophobicity in order to provide a more physically realistic model of the interaction at nanometer-scale separation distances.

Acknowledgements

This research was supported by Vaadia-BARD Postdoctoral Fellowship Award No. FI-435-2010 from BARD, The United States – Israel Binational Agricultural Research and Development Fund.

Appendix A. Higher-order terms in the asymptotic approximation

The set of perturbation equations formulated in Section 2.1 may be generally written as:

$$\frac{1}{12\eta}\frac{d}{d\eta}\left(\eta H^3\frac{dP_n}{d\eta}\right) - P_{n-1} = 0, \quad n \geq 1, \tag{A.1}$$

correcting the base solution of a non-permeable wall to account for permeability effects.

Solving sequentially for higher orders up to $O(\alpha^6)$, the additional terms for the pressure field are as follows:

$$P_2 = \frac{\left(168\Delta + 48\eta^2\right)\alpha^2}{\Delta^3 H^4},$$

$$P_3 = -\frac{\left(2808\Delta^2 + 1980\Delta\eta^2 + 360\eta^4\right)\alpha^3}{5\Delta^5 H^5},$$

$$P_4 = \frac{144\left(321\Delta^3 + 378\Delta^2\eta^2 + 150\Delta\eta^4 + 20\eta^6\right)\alpha^4}{25\Delta^7 H^6},$$

$$P_5 = -\frac{36}{175\Delta^9 H^7}(29448\Delta^4 + 49140\Delta^3\eta^2 + 30870\Delta^2\eta^4 + 8645\Delta\eta^6 + 910\eta^8)\alpha^5,$$

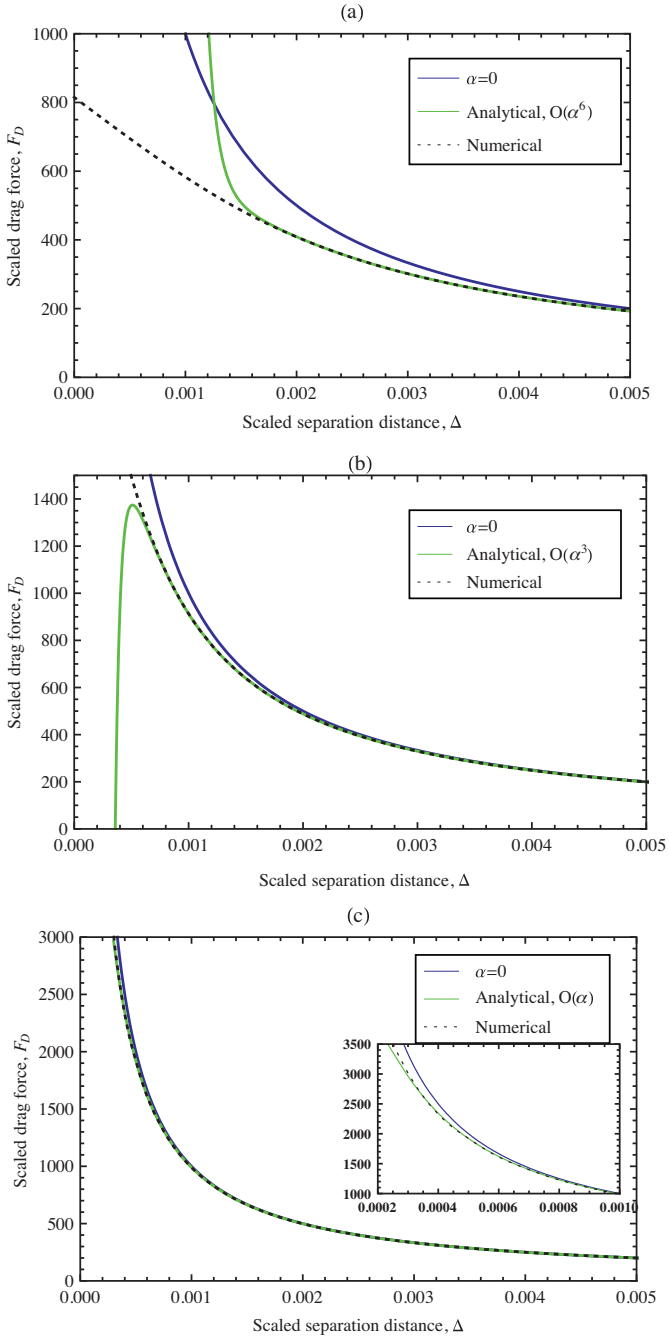

Fig. B.1. Scaled force, F_D as a function of separation, Δ, calculated using the numerical solution and the analytical solution at various degrees of approximation. (a) $\alpha = 10^{-6}$, (b) $\alpha = 10^{-7}$, and (c) $\alpha = 10^{-8}$. Inset: enlarged view at close separation, showing the deviation of the permeable wall case from the impermeable case.

$$P_6 = \frac{54}{1225\Delta^{11}H^8}(449576\Delta^5 + 973760\Delta^4\eta^2 + 844760\Delta^3\eta^4 + 366800\Delta^2\eta^6 + 79695\Delta\eta^8 + 6930\eta^{10})\alpha^6.$$

The following additional terms have been calculated for the drag force, F_D, which may be added to the $O(\alpha)$ approximation, Eq. (22), for increased accuracy at close approach:

$$F_{D,2} = \frac{3\alpha^2}{2\Delta^5}, \quad F_{D,3} = -\frac{12\alpha^3}{5\Delta^7}, \quad F_{D,4} = \frac{39\alpha^4}{10\Delta^9},$$

$$F_{D,5} = -\frac{891\alpha^5}{140\Delta^{11}}, \quad F_{D,6} = \frac{5823\alpha^6}{560\Delta^{13}},$$

where all terms are multiplied by a factor $6\pi(V_s - 1)$, and the added subscript is to be understood as the order of the respective term in the asymptotic expansion.

Appendix B. Accuracy of the approximations at various orders

Some representative calculations illustrating the accuracy of the analytical solution at various orders of approximation are plotted in Fig. B.1, and the absolute deviation (in %) of the analytical solution from the numerical one is illustrated in Fig. B.2. Higher permeabilities and closer separation require more terms to be added in the series expansion for increased accuracy. For example, at a permeability of $\alpha = 10^{-5}$, the analytical solution at $O(\alpha^6)$ is accurate up to a separation of $\Delta \approx 0.005$, while at $\alpha = 10^{-8}$ the first order correction is sufficiently accurate up to a separation of $\Delta \approx 0.0002$.

In order to better illustrate the applicability of the derived solution, Table B.1 summarizes the range of separation distances for which the analytical approximation is within 1% of the numerical calculations, for different permeabilites and orders of approximation. It may be concluded that the approximation may be used to calculate the force for many practical cases of interest in membrane separation processes. If corrected for large separations by adding the Stokes equation, the drag on a sphere may henceforth be easily calculated using closed-form expressions. Furthermore, the numerical solution of the derived Eq. (14) is considerably more straightforward than is the solution of the system of difference equations resulting from the full stream-function analysis.

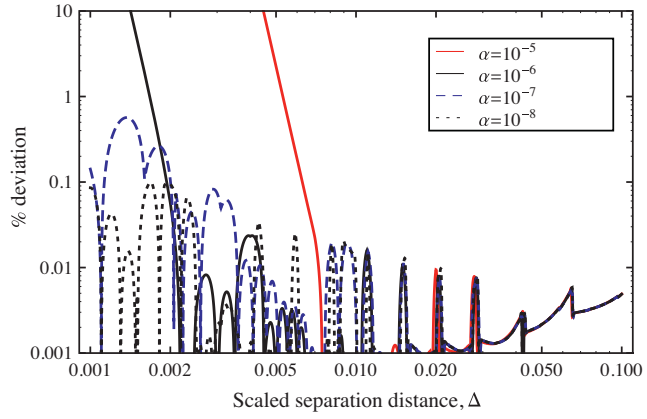

Fig. B.2. Absolute value of the deviation (%) of the analytical solution, at $O(\alpha^6)$, from the numerical solution, calculated for various scaled permeabilities.

Table B.1
Range of parameters corresponding to a 1% deviation between the analytical and numerical calculations.

	Range of accuracy, Δ>		
α	$O(\alpha^6)$	$O(\alpha^3)$	$O(\alpha)$
10^{-5}	0.0054	0.0065	0.011
10^{-6}	0.0017	0.0021	0.0035
10^{-7}	0.0006	0.0007	0.0011
10^{-8}	0.0002	0.0003	0.00032

Nomenclature

F_D	scaled drag force [–]
h	gap width [m]
H	scaled gap width, h/R [–]
k	specific Darcy permeability [m]
p	pressure [Pa]
p_∞	background pressure [Pa]
R	particle radius [m]
r	radial coordinate [m]
v	permeation velocity [m/s]
v_s	velocity of the sphere [m/s]
V_s	scaled sphere velocity [–]
z	transverse coordinate [m]

Greek letters

α	scaled permeability, k/R [–]
η	scaled radial coordinate, r/R [–]
δ	separation distance [m]
Δ	scaled separation distance, δ/R [–]
μ	viscosity [kg/(m s)]

References

[1] H. Brenner, The slow motion of a sphere through a viscous fluid towards a plane surface, Chem. Eng. Sci. 16 (3–4) (1961) 242–251.

[2] A. Goldman, R. Cox, H. Brenner, Slow viscous of a sphere parallel to a plane wall, 1-motion through a quiescent fluid, Chem. Eng. Sci. 22 (1967) 637–651.

[3] S.L. Goren, The hydrodynamic force resisting the approach of a sphere to a plane permeable wall, J. Colloid Interface Sci. 69 (1) (1979) 78–85.

[4] Z. Yan, S. Weinbaum, R. Pfeffer, The three-dimensional hydrodynamic interaction of a finite sphere with a circular orifice at low Reynolds number, J. Fluid Mech. 179 (1987) 39–68.

[5] R.P.J.N. Kao, Y. Wang, S. Weinbaum, A theoretical model for nucleopore filters including hydrodynamic and molecular wall interaction effects, J. Colloid Interface Sci. 121 (2) (1988) 543–557.

[6] W. Wu, S. Weinbaum, A. Acrivos, Shear flow over a wall with suction and its application to particle screening, J. Fluid Mech. 243 (1992) 489–518.

[7] J. Lin, D. Bourrier, M. Dilhan, P. Duru, Particle deposition onto a microsieve, Phys. Fluids 21 (2009) 073301.

[8] S. Chellam, M.R. Wiesner, Particle transport in clean membrane filters in laminar flow, Environ. Sci. Technol. 26 (8) (1992) 1611–1621.

[9] J.S. Knutsen, R.H. Davis, Deposition of foulant particles during tangential flow filtration, J. Membr. Sci. 271 (1–2) (2006) 101–113.

[10] S. Kang, A. Subramani, E.M.V. Hoek, M.A. Deshusses, M.R. Matsumoto, Direct observation of biofouling in cross-flow microfiltration: Mechanisms of deposition and release, J. Membr. Sci. 244 (1–2) (2004) 151–165.

[11] S. Wang, G. Guillen, E.M.V. Hoek, Direct observation of microbial adhesion to membranes, Environ. Sci. Technol. 39 (17) (2005) 6461–6469.

[12] S. Kim, M. Marion, B. Jeong, E.M.V. Hoek, Crossflow membrane filtration of interacting nanoparticle suspensions, J. Membr. Sci. 284 (1–2) (2006) 361–372.

[13] A. Subramani, E.M.V. Hoek, Direct observation of initial microbial deposition onto reverse osmosis and nanofiltration membranes, J. Membr. Sci. 319 (1–2) (2008) 111–125.

[14] L.G. Leal, Advanced Transport Phenomena: Fluid Mechanics and Convective Transport Processes, Cambridge University Press, 32 Avenue of the Americas, NY 10013-2473, USA, 2007.

[15] A. Oron, S.H. Davis, S.G. Bankoff, Long-scale evolution of thin liquid films, Rev. Mod. Phys. 69 (3) (1997) 931–980.

[16] E. Bonaccurso, H. Butt, V.S.J. Craig, Surface roughness and hydrodynamic boundary slip of a Newtonian fluid in a completely wetting system, Phys. Rev. Lett. 90 (14) (2003) 144501/1–144501/4.

[17] N. Lecoq, R. Anthore, B. Cichocki, P. Szymczak, F. Feuillebois, Drag force on a sphere moving towards a corrugated wall, J. Fluid Mech. 513 (2004) 247–264.

[18] C.L. Henry, V.S.J. Craig, Measurement of no-slip and slip boundary conditions in confined Newtonian fluids using atomic force microscopy, Phys. Chem. Chem. Phys. 11 (41) (2009) 9514–9521.

[19] C. Kunert, J. Harting, O.I. Vinogradova, Random-roughness hydrodynamic boundary conditions, Phys. Rev. Lett. 105 (1) (2010) 016001.

[20] J.O. Marston, W. Yong, S.T. Thoroddsen, Direct verification of the lubrication force on a sphere travelling through a viscous film upon approach to a solid wall, J. Fluid Mech. 655 (2010) 515–526.